Projectile fragmentation of radioactive beams of ^{68}Ni, ^{69}Cu, and ^{72}Zn

S. Lukyanov,[1,2,*] M. Mocko,[1,3,4] L. Andronenko,[1,5] M. Andronenko,[1,5,†] D. Bazin,[1] M. A. Famiano,[1,6] A. Gade,[1] S. P. Lobastov,[1,2] W. G. Lynch,[1,4] A. M. Rogers,[1,4] O. B. Tarasov,[1,2] M. B. Tsang,[1,4] G. Verde,[1,7] M. S. Wallace,[1,3] and R. G. T. Zegers[1,4]

[1]*National Superconducting Cyclotron Laboratory, Michigan State University, East Lansing, Michigan 48824, USA*
[2]*Flerov Laboratory of Nuclear Reactions, Joint Institute for Nuclear Research, RU-141980 Dubna, Moscow region, Russian Federation*
[3]*Los Alamos National Laboratory, Los Alamos, New Mexico 87545, USA*
[4]*Department of Physics & Astronomy, Michigan State University, East Lansing, Michigan 48824, USA*
[5]*PNPI, Gatchina, Leningrad district RU-188300, Russian Federation*
[6]*Department of Physics, Western Michigan University, Kalamazoo, Michigan 49008, USA*
[7]*INFN, Sezione di Catania, 64 Via Santa Sofia, I-95123 Catania, Italy*

(Received 21 April 2009; published 14 July 2009)

The fragment production cross sections of secondary neutron-rich beams of ^{68}Ni, ^{69}Cu, and ^{72}Zn isotopes at energies of about 95*A* MeV have been measured. We compare the measured cross sections to EPAX, an empirical parametrization of fragmentation cross sections. A reasonable agreement of the experimental data and EPAX predictions suggests that an EPAX parametrization used for stable beams seems to be valid for unstable neutron-rich ion beams. EPAX tends to overestimate the yields of neutron-rich isotopes. This problem is amplified when neutron-rich radioactive beams are employed, leading to overly optimistic estimates of the production of neutron-rich isotopes.

DOI: 10.1103/PhysRevC.80.014609 PACS number(s): 25.70.Mn, 25.60.Dz

I. INTRODUCTION

The availability of radioactive ion beams has broadened the study of nuclear structure and nuclear reactions [1]. One of the most efficient ways to produce rare isotopes is via projectile fragmentation [2–4]. As the exact reaction mechanism of the projectile fragmentation is not well understood [5–10], phenomenological parametrizations such as EPAX [11] are widely used to estimate rates at current radioactive beam facilities [1]. EPAX provides reasonably accurate rates for production of nuclei close to the valley of stability. However, problems emerge when these predictions are extended to the neutron-rich extremes of the secondary beams [5–10]. This issue becomes particularly important when one wants to predict how the yield of a given rare isotope depends on the choice of the primary beam, an important consideration in designing experiments at rare-isotope-beam facilities. It is also very important, for example, to calculate beam rates using high-energy primary beams where thick targets are used. In such cases, calculations have shown that multiple interactions in the target may be the dominant contributor of rare isotopes, and thus it may be essential to describe thick target data [2]. To make predictions for contributions from two and multisteps [10], it has been assumed that EPAX predictions are the correct description for the contribution from single interactions, even for fragmentation of unstable nuclei. The aim of this study is to test this assumption with radioactive beams of ^{68}Ni, ^{69}Cu, and ^{72}Zn.

II. EXPERIMENTAL SETUP

Fragmentation experiments with ^{64}Ni, ^{68}Ni, ^{69}Cu, and ^{72}Zn beams were performed at the National Superconducting Cyclotron Laboratory (NSCL) at Michigan State University (MSU). A schematic layout of the experimental setup is shown on Fig. 1. The beam energy and intensity of the secondary beams are summarized in Table I. To produce these beams, a 131-*A* MeV primary beam of ^{76}Ge was accelerated and struck a 245 mg/cm^2 thick beryllium production target. The average intensity of the ^{76}Ge beam during the experiment was about 200 electrical nanoAmpere corresponding to 6.3×10^{10} pps. Secondary beams of ^{64}Ni, ^{68}Ni, ^{69}Cu, and ^{72}Zn ions were selected with the A1900 fragment separator [12]. A wedge made of 250 mg/cm^2 thick aluminum foil, located at the intermediate image of the A1900 fragment separator, was used to minimize the amount of contaminant species in the beams [13].

Produced fragments were detected with the high-resolution magnetic spectrometer S800 [13], which was specially designed for reaction studies with radioactive beams. To cross-check our experimental setup, and to understand the transmission characteristics of the S800 spectrometer, we measured the cross sections of fragments produced by the ^{64}Ni beam, which was delivered as a secondary beam in the present experiment. The fragmentation of ^{64}Ni, produced as a stable beam at 140*A* MeV on a beryllium target, has been measured previously [6] at the Coupled Cyclotron Facility at NSCL using the A1900 fragment separator. Thus, the fragment cross sections measured in the present work with the ^{64}Ni secondary beam can be compared to the cross sections obtained with the ^{64}Ni primary beam [6].

Three different magnetic settings in the A1900 fragment separator were used to optimize the production of ^{64}Ni beam, ^{72}Zn beam, and the cocktail beams of ^{68}Ni and ^{69}Cu. In each case, other contaminant ions with the same mass-to-charge ratios were present. Software gates must be applied to ensure that the detected fragments were produced from the interaction of a specific beam with the secondary target. Identification of secondary beams was made by measuring the energy

*Corresponding author: lukyan@nrmail.jinr.ru
†Deceased.

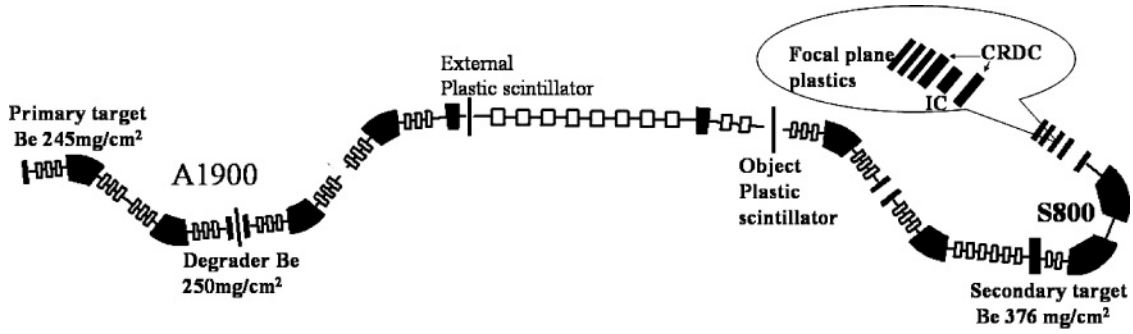

FIG. 1. Schematic of the A1900 [12] and S800 [13] spectrometers.

loss of the beam, ΔE, in the plastic scintillator, which is part of the S800 focal plane detection system, and the time of flight, ToF, between two plastic scintillator detectors located in the external focal plane of the A1900 fragment separator and in the object image plane of the S800 spectrometer. A two-dimensional spectrum showing yields as a function of ToF and ΔE is given in the top panel of Fig. 2, which shows that both ^{68}Ni and ^{69}Cu beams are cleanly separated. The relative intensity of the beams can be obtained by projecting the counts on the ToF axis (bottom panel). All analyzed events have the appropriate beam gate on spectra similar to Fig. 2.

The large acceptance of the S800 spectrograph both in solid angle (20 msr) and momentum ($\mathrm{d}p/p \sim 5.4\%$) are well matched with the large emittance of the secondary beams produced by projectile fragmentation. The fragment cross sections have been measured between magnetic settings of 2.53 and 3.02 Tm for ^{68}Ni and ^{69}Cu beams and between 2.45 and 3.02 Tm for the ^{72}Zn beam. For each reaction, only five to eight settings of magnetic rigidity are needed. The reaction target, a 376 mg/cm^2 thick beryllium foil, was placed inside the scattering chamber in the S800 beam line (Fig. 1). The emitted fragments were collected and identified in the focal plane of the S800. The focal plane detection system consists of a pair of cathode readout drift chambers (CRDCs) located about 1 m apart, followed by a multisegmented ion chamber (IC) and four large focal-plane plastic scintillators of thicknesses of 3 mm, 5 cm, 10 cm, and 20 cm, respectively [13]. The active area covered by these detectors is about 60×30 cm^2. The CRDCs provide a measurement of position and angle in both dispersive and nondispersive planes.

The standard identification method of the fragments based on the magnetic rigidity ($B\rho$), ToF, and ΔE values was used on an event-by-event basis. The ToF was measured by requiring a coincidence between the object plastic scintillator of the S800 and the plastic scintillator located at the focal plane of the S800 spectrometer. Energy loses of fragments were measured with the ion chamber at the S800 focal plane. From the charge state distribution simulation using the code GLOBAL [14] implemented in LISE++ [15], we expect less than a 1% contribution from hydrogen-like charge states for all projectiles on a beryllium target. By assuming that all fragments were fully stripped of their electrons ($Q = Z$), the $B\rho$-ToF-ΔE method [6] is sufficient for the identification of the detected fragments in the present experiment. An example of fragment identification is shown on Fig. 3. The accuracy in the Z and $N - Z$ determination was about 0.55 (FWHM) units for the fragments in the region of $17 \leqslant Z \leqslant 31$.

The momentum of the detected fragments can be deduced from the fragment position in the dispersive plane using the $B\rho$ rigidity:

$$B\rho[\mathrm{Tm}] = B\rho_0\{1 + x/(D \times 100)\}, \qquad (1)$$

TABLE I. Summary of the properties of the secondary beams used in the present experiment.

Projectile	^{64}Ni	^{69}Cu	^{72}Zn	^{68}Ni
Purity of the secondary beam (%)	∼80	∼60	∼95	∼30
Beam N/Z ratio	1.29	1.38	1.40	1.43
Energy (A MeV)	93.7	98.1	95.4	94.3
Mean intensity (pps)	7.1×10^4	5.0×10^4	7.0×10^4	2.2×10^4

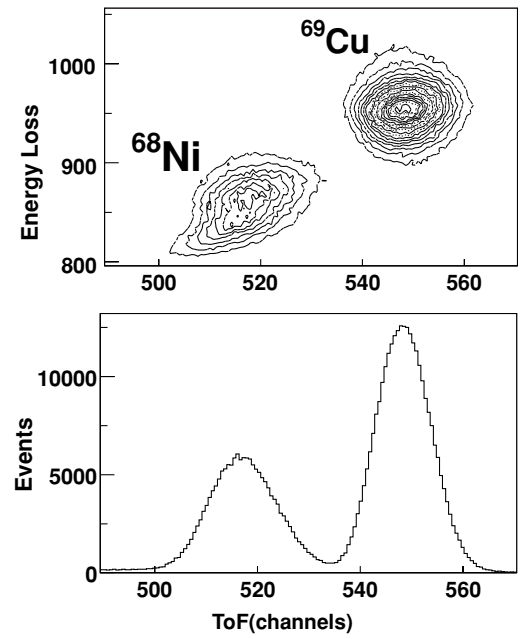

FIG. 2. (Top) Secondary beam particle identification from the two-dimensional spectrum of energy loss in a plastic detector versus ToF. (Bottom) Projection onto the ToF axis.

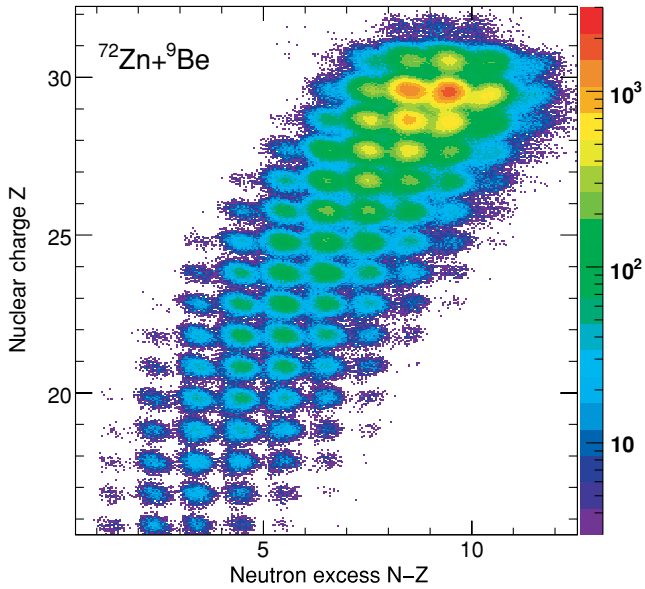

FIG. 3. (Color online) Particle identification spectrum obtained in the ^{72}Zn + ^{9}Be reaction. In this representation, the ΔE and ToF signals have been calibrated and converted to Z and $N - Z$.

where $B\rho_0$, given by the magnetic rigidity setting of the S800, corresponds to the $B\rho$ for the central trajectory of fragments, x is the coordinate in the dispersive plane measured by the CRDCs, and $D = 9.5$ cm/% is the dispersion value of the S800 spectrometer. Momentum distributions of the identified fragments were determined from the position spectra of the CRDCs, according to Eq. (1). In the analysis of the present experiment, we use a bin size of 1 cm in the x position, corresponding to 0.1% accuracy in the $B\rho$ determination. Three examples of the momentum distribution are shown in Fig. 4 for the fragments of ^{47}Ca, ^{54}V, and ^{62}Co, produced in the fragmentation reaction of ^{72}Zn + ^{9}Be. The differential cross sections, $d\sigma/dp(A, Z)$, for a fragment with mass number A and proton number Z were calculated by taking into account the number of beam particles, N_B, the number of target nuclei per square centimeter, N_T, the live-time ratio, τ_{LIVE}, and the transmission efficiency through the S800 spectrometer, ε,

$$\frac{d\sigma}{dp}(A, Z) = \frac{N(A, Z)}{N_T N_B \Delta p \tau_{\mathrm{LIVE}}} \frac{1}{\varepsilon}, \tag{2}$$

where $N(A, Z)$ is the number of fragments detected within the momentum bin Δp. Unlike the momentum distributions obtained in Ref. [6], the momentum distributions obtained in the present experiment are nearly symmetric. The difference probably arises from the thicker target and wider momentum acceptance of the secondary beams used in the present experiment. The target was nearly three times thicker and the momentum spread (0.5%) of the secondary beams was 2.5 times larger than the target and momentum coverage in the earlier experiment [6].

The momentum distributions are fitted with a Gaussian function,

$$\frac{d\sigma}{dp} = C \exp\left[-(p - p_0)^2 / 2\sigma_0^2\right], \tag{3}$$

where C is the normalization factor and p_0 and σ_0 correspond to the peak position and width of the Gaussian fit of the momentum distribution.

The transmission coefficient, ε, is determined by comparing the dispersive and nondispersive angular distributions. The fragment angular distributions were reconstructed with the inverse mapping technique. The inverse map relates the positions and angles measured in the focal plane in both dispersive and nondispersive planes at the target position. This method uses the ion optics code COSY Infinity [16] to calculate the aberrations to an arbitrary order, inverts the obtained polynomial matrix, and then applies the corrections on event-by-event basis in the analysis software.

Figure 5 shows the dispersive angular distributions at the target positions for ^{44}Ca and ^{59}Co fragments of the ^{64}Ni + ^{9}Be reaction at 93.7A MeV. As expected, the angular distributions in the dispersive plane have a symmetric Gaussian-like shape. The measured distribution in the nondispersive plane had asymmetric shapes because of misalignment of the S800 spectrometer, which was discovered after the experiment. The transmission coefficient, ε, was derived from the ratios of the area of a fitted Gaussian function of nondispersive

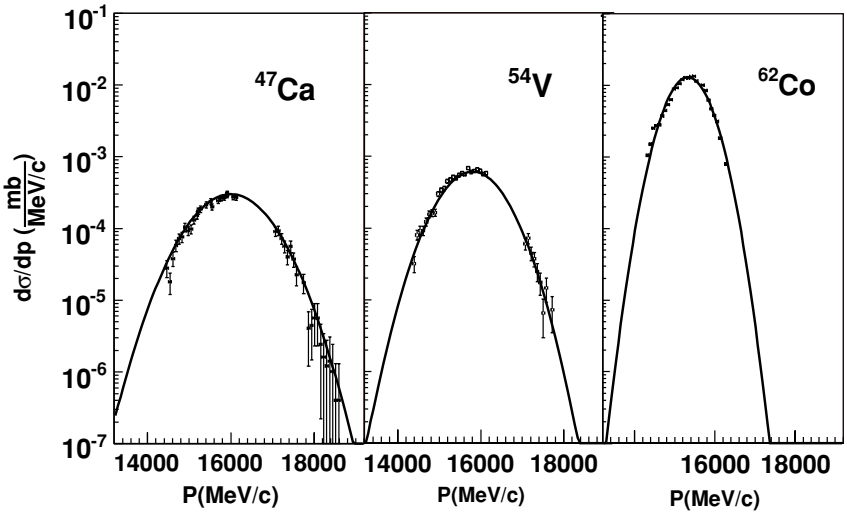

FIG. 4. Momentum distributions for fragments ^{47}Ca, ^{54}V, and ^{62}Co produced in fragmentation of ^{72}Zn on a ^{9}Be target. The solid curves represent Gaussian fits.

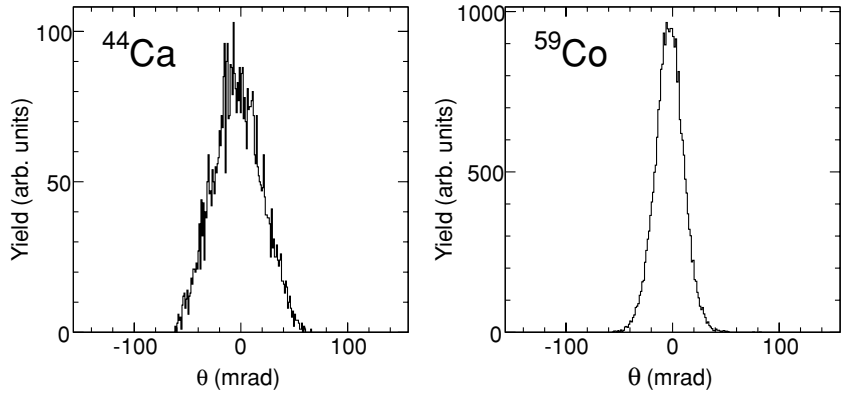

FIG. 5. Dispersive angular distributions at the target position for ^{44}Ca and ^{59}Co fragments from the ^{64}Ni + ^{9}Be reactions at 93.7A MeV, measured at the S800 spectrograph using an inverse map calculation (see text).

angular distribution to the counts obtained in the dispersive angular distribution. The extracted transmission, ε, which is proportional to the difference between the atomic number of the projectile, A_p, and that of the detected fragment mass, A_f, ranges from 0.7 for argon fragments to 1.0 for fragments close to the projectile, $A_p - A_f < 3$.

III. CROSS-SECTION MEASUREMENTS

The fragment cross sections were determined by integrating the area of their momentum distributions. Unfortunately, not all fragments have measured momentum distributions such as those shown in Fig. 4. More than 40% of the detected fragments had incomplete measured momentum distributions, which may consist of only slightly more than half of the momentum distribution or, in some cases, only a few data points near the top of the peak. For these fragments, we used the procedure described in Ref. [6], where p_0 is parametrized as a linear function of the mass fragments to extrapolate the centroids of the incompletely measured momentum distributions. To check our method, the fragment cross sections for ^{64}Ni + ^{9}Be at 93.7A MeV are compared with fragmentation data of ^{64}Ni [6] at 140A MeV (Fig. 6). Each panel in Fig. 6 represents isotope cross-section data for one element, plotted as a function of neutron excess, $N - Z$, of each isotope. Filled circles represent fragmentation data measured in the present work and open circles represent measured cross sections from Ref. [6].

Reasonable agreement between the two sets of data at different projectile energies shows that the fragmentation reaction is relatively insensitive to the incident energy around 100A MeV. The disagreements between the two measurements for the most proton rich isotopes may arise from the inaccurate extrapolations of cross sections from incomplete momentum distributions measured in the present experiment. For reference, the results of the EPAX [11] calculation are shown as solid curves in Fig. 6.

The fragmentation-production cross sections measured for reactions ^{68}Ni + Be, ^{69}Cu + Be, and ^{72}Zn + Be are reported in Figs. 7, 8, and 9, respectively. In these figures, the closed squares represent fragmentation data with complete momentum distribution measurements, and the open squares represent fragmentation data with incomplete momentum distributions. Owing to low intensity of secondary beams, we were able to cover only three orders of magnitude in cross section, reaching the minimum cross sections at 0.1 mb for ^{68}Ni and 0.01 mb for ^{72}Zn beams, respectively. The solid curves are predictions from EPAX. The overall agreement between EPAX and the data is similar to that obtained from the fragmentation of stable beams of ^{58}Ni and ^{64}Ni [6]. The reasonable quantitative description of the experimental data obtained from the fragmentation of secondary beams indicates that the parametrization derived from stable beams is valid for the case of unstable neutron-rich ions at beam energies around 100A MeV. Our observation is consistent with fragment distributions obtained for neutron-rich oxygen beams [17] and

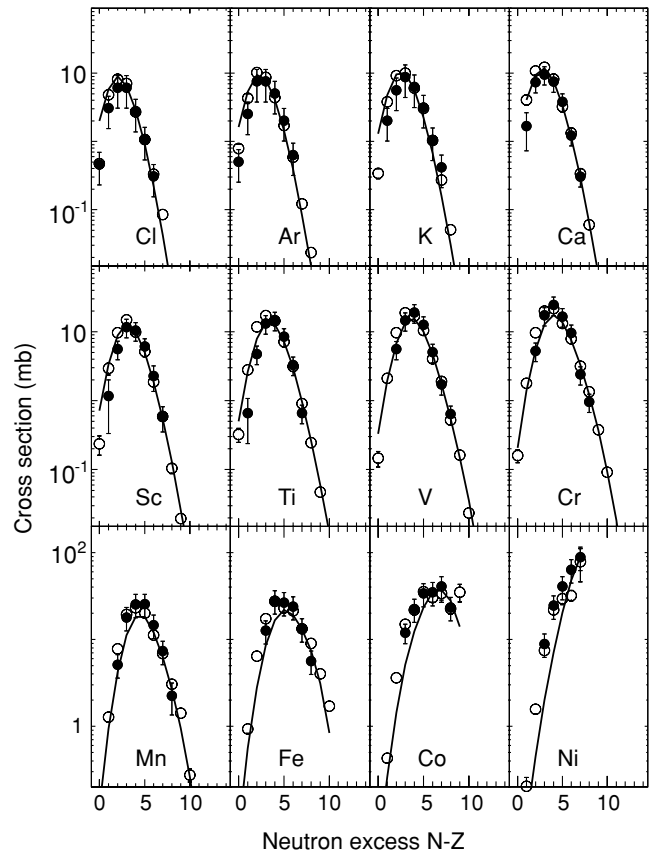

FIG. 6. Cross sections plotted as a function of neutron excess, $N - Z$, for the fragmentation reaction of ^{64}Ni at 93.7A MeV, on a beryllium target (solid circles) in comparison with data from ^{64}Ni + ^{9}Be reactions at 140A MeV (open circles) [5].

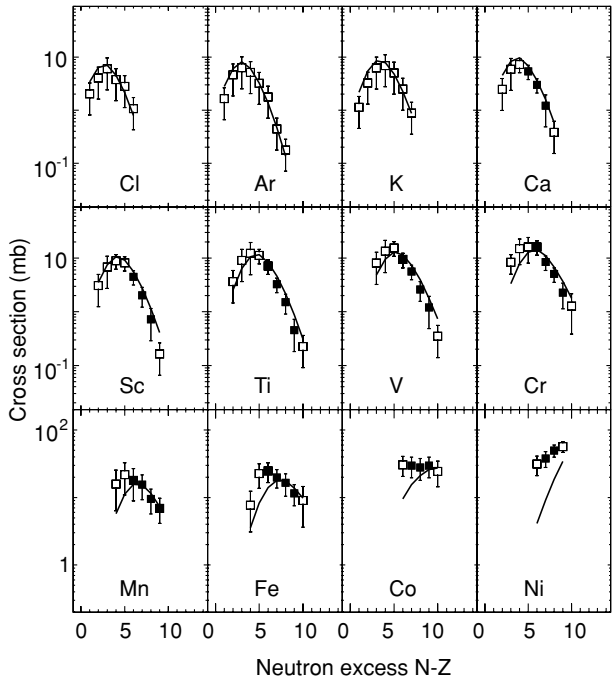

FIG. 7. Isotope distributions for Ca–Ni elements detected in reaction with a ^{68}Ni beam at 94.3A MeV. Experimental fragmentation data are shown as filled squares (complete momentum distribution measurement) and open squares (incomplete momentum distribution measurement). EPAX predictions are shown as solid lines.

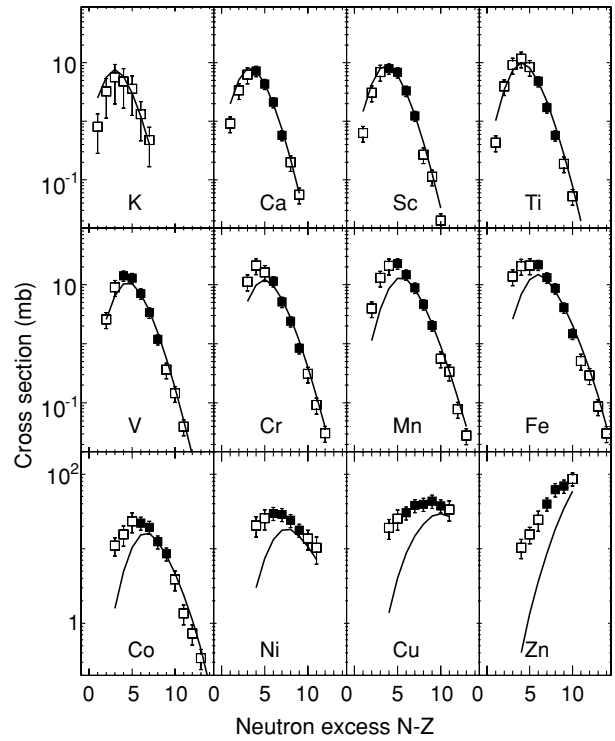

FIG. 9. Isotope distributions for K–Zn elements detected in reaction with a ^{72}Zn beam at 95.4 A MeV. We use the same symbol conventions as in Fig. 7.

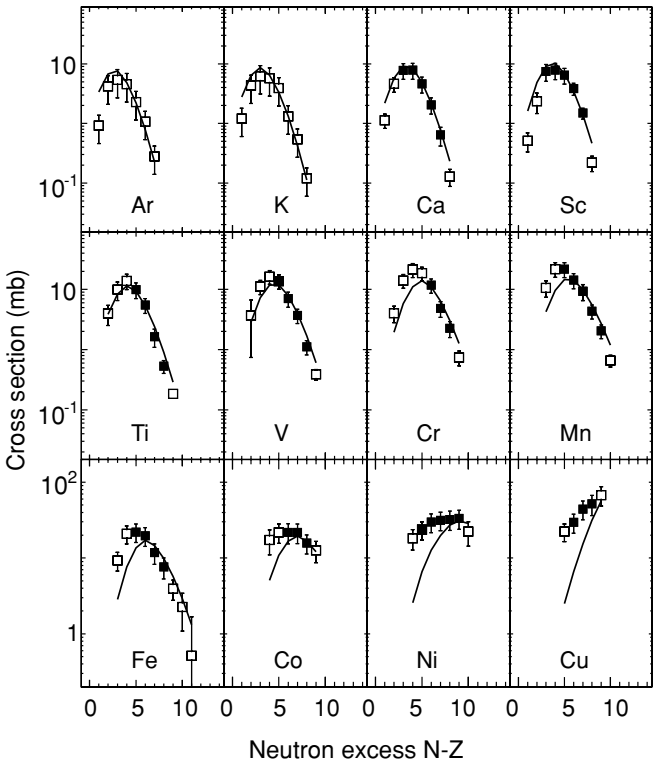

FIG. 8. Isotope distributions for Ar–Cu elements detected in reaction with a ^{69}Cu beam at 98.1A MeV. We use the same symbol conventions as in Fig. 7.

for the neutron-deficient ^{36}Ar isotope [18]. Until results from a more accurate model on projectile fragmentation reactions are available, current comparisons of our data to the EPAX code suggest that there is no appreciable difference in the reaction mechanisms of the projectile fragmentation of neutron-rich unstable and stable beams.

The disagreement between measured cross sections and EPAX predictions for projectile-like fragments close to the valley of stability (see the region of Mn–Ni fragments in Figs. 7–9) increases with the neutron richness of the projectiles. Such an observation is consistent with previous fragmentation cross-section results from neutron-rich (^{48}Ca, ^{64}Ni, and ^{86}Kr) and neutron-poor (^{40}Ca and ^{58}Ni) stable beams [6].

Figure 10 shows the comparison of the production cross sections for isotopes from calcium to nickel produced from the fragmentation of different nickel isotopes. The peak of the isotope production cross section decreased with an increase of the neutron excess of the projectile. Whereas the peak positions of the isotope distributions shift to more neutron-rich isotopes with increasing neutron richness of the projectile, the shift is not proportional to the neutron excess difference of the projectiles. For instance, the centroids of the chromium isotope distributions for ^{58}Ni to ^{68}Ni projectiles only shift by about 2–3 mass units. The relatively small shift in the peak position of the isotope distributions can be understood as the neutron-rich prefragments created in the fragmentation process decay toward the valley of stability. However, the widths of the isotope distributions increase with the neutron richness of the beams.

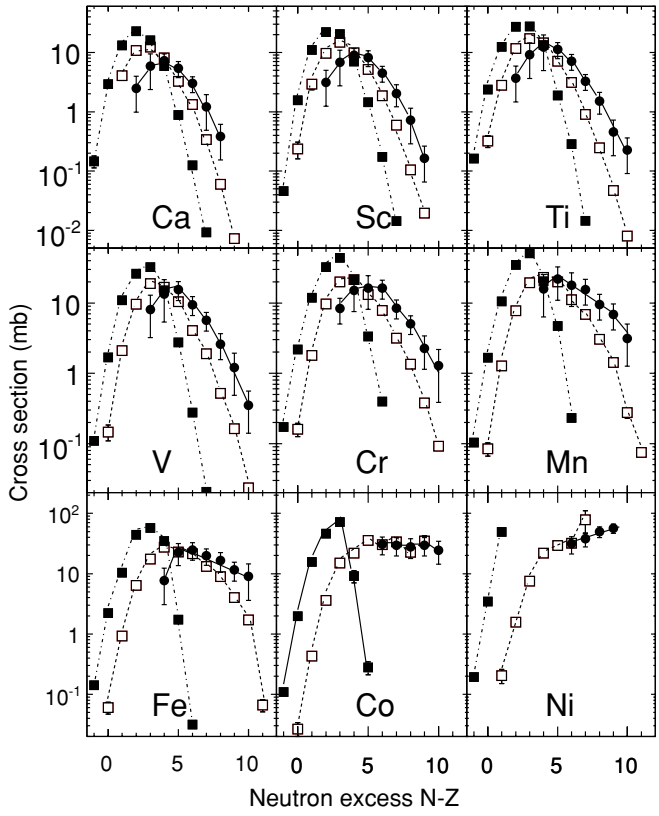

FIG. 10. Isotope distributions from the fragmentation of 140-*A* MeV ^{58,64}Ni [5,7] (solid and open squares) and 94.3-*A* MeV ^{68}Ni (solid circles) with a beryllium target. Lines are drawn to guide the eye.

As expected, the gain in fragment production is greater for the production of very neutron-rich isotopes using the neutron-rich beams. Unfortunately, the gain does not compensate for the severe limitations in beam intensities of secondary beams compared to neutron-rich primary beams such as ^{86}Kr. Thus, production of neutron-rich rare-isotope beams using fragmentation secondary beams may not be practical, except for the very neutron-rich nuclei near the drip line.

IV. SUMMARY

In summary, we measured fragmentation of secondary beams of neutron-rich ^{68}Ni, ^{69}Cu, and ^{72}Zn isotopes at energies of about 95 *A* MeV. The cross sections were obtained by integrating the momentum distributions of isotopes with $Z \geqslant 17$ measured in the S800 spectrometer. We compared the measured cross sections to EPAX results. The quantitative description of experimental data for the fragmentation of secondary beams of ^{68}Ni, ^{69}Cu, and ^{72}Zn indicates that a parametrization used for stable beams is valid for unstable neutron-rich ion beams. The results suggest that the reaction mechanisms in the projectile fragmentation of unstable beam are very similar to those of stable beams.

ACKNOWLEDGMENTS

Our sincere gratitude is extended to the staff members of the NSCL coupled cyclotron facility for their assistance in providing the beams for the experiment. This work is supported by the National Science Foundation under Grant Nos. PHY-01-10253, PHY-0606007, INT-0218329, and DE-FG02-04ER41313. SL acknowledges partial support from Michigan State University during his stay at the NSCL.

[1] *Scientific Opportunities with a Rare-Isotope Facility in the United States* (National Academies Press, Washington, 2007).
[2] H. Geissel *et al.*, Nucl. Instrum. Methods Phys. Res. B **70**, 286 (1992).
[3] T. Kubo, M. Ishihara, N. Inabe, H. Kumagai, I. Tanihata, and K. Yoshida, Nucl. Instrum. Methods Phys. Res. B **70**, 309 (1992).
[4] B. M. Sherrill, Prog. Theor. Phys. Suppl. **146**, 60 (2002).
[5] M. Mocko *et al.*, Europhys. Lett. **79**, 12001 (2007).
[6] M. Mocko *et al.*, Phys. Rev. C **74**, 054612 (2006).
[7] M. Mocko *et al.*, Phys. Rev. C **76**, 014609 (2007).
[8] M. B. Tsang *et al.*, Phys. Rev. C **76**, 041302(R) (2007).
[9] M. Notani *et al.*, Phys. Rev. C **76**, 044605 (2007).
[10] W. A. Friedman and M. B. Tsang, Phys. Rev. C **67**, 051601(R) (2003).
[11] K. Sümmerer and B. Blank, Phys. Rev. C **61**, 034607 (2000).
[12] A. Stolz, T. Baumann, T. N. Ginter, D. J. Morrissey, M. Portillo, B. M. Sherrill, M. Steiner, and J. W. Stetson, Nucl. Instrum. Methods Phys. Res. B **241**, 858 (2005).
[13] D. Bazin, J. A. Caggiano, B. M. Sherrill, J. Yurkon, and A. Zeller, Nucl. Instrum. Methods Phys. Res. B **204**, 629 (2003).
[14] C. Scheidenberger, T. Stöhlker, W. E. Meyerhof, H. Geissel, P. H. Mokler, and B. Blank, Nucl. Instrum. Methods Phys. Res. B **142**, 441 (1998).
[15] D. Bazin, O. Tarasov, M. Lewitowicz, and O. Sorlin, Nucl. Instrum. Methods Phys. Res. A **482**, 307 (2002), http://www.nscl.msu.edu/lise.
[16] http://bt.pa.msu.edu/index_cosy.htm.
[17] A. Leistenschneider *et al.*, Phys. Rev. C **65**, 064607 (2002).
[18] M. Caamano, D. Cortina-Gil, K. Sümmerer, J. Benlliure, E. Casarejos, H. Geissel, G. Münzenberg, and J. Pereira, Nucl. Phys. **A733**, 187 (2004).